Contrib Mineral Petrol (2000) 139: 36–53

J. A. Pearce · P. F. Barker · S. J. Edwards
I. J. Parkinson · P. T. Leat

Geochemistry and tectonic significance of peridotites from the South Sandwich arc–basin system, South Atlantic

Received: 31 August 1999 / Accepted: 3 December 1999

Abstract Petrographic and geochemical studies of peridotites from the South Sandwich forearc region provide new evidence for the evolution of the South Sandwich arc–basin system and for the nature of interactions between arc magma and oceanic lithosphere. Peridotites from the inner trench wall in the north-east corner of the forearc vary from clinopyroxene-bearing harzburgites, through samples transitional between harzburgites and dunites or wehrlites, to dunites. The harzburgites are LREE depleted with low incompatible element abundances and have chromites with intermediate Cr# (ca. 0.40). Modelling shows that they represent the residues from 15–20% melting at oxygen fugacities close to the QFM buffer. The dunites have U-shaped REE patterns, low incompatible element abundances and high Cr# (0.66–0.77). Petrography and geochemistry indicate that the latter are the product of intense interaction between peridotite and melt saturated with olivine under conditions of high oxygen fugacity (QFM + 2). The transitional samples are the product of lesser interaction between peridotite and melt saturated with olivine ± clinopyroxene. The data demonstrate that the harzburgites originated as the residue from melting at a ridge (probably the early East Scotia Sea spreading centre), and were subsequently modified to transitional peridotites and dunites by interaction with South Sandwich arc magmas. The second dredge locality, near the South Sandwich Trench–Fracture Zone intersection, yielded rocks ranging from lherzolite to harzburgite that could similarly have resulted from a two-stage melting and enrichment process, but involving a more fertile mantle residue and a reacting melt that is transitional between MORB and island arc tholeiite. The South Sandwich peridotites have a similar petrogenetic history to those from Conical Seamount in the Mariana forearc in the sense that both involved interaction between arc magma and pre-existing mantle lithosphere of different provenance. However, the precise compositions of the magma and mantle components vary from location to location according to the precise tectonic setting and tectonic history. Overall, therefore, data from the South Sandwich and Izu–Bonin–Mariana systems emphasise the potential significance of peridotite geochemistry in unravelling the complex tectonic histories of forearcs past and present.

J. A. Pearce[1] (✉)
Department of Geological Sciences, University of Durham, Durham DH1 3LE, UK

P. F. Barker · P. T. Leat
British Antarctic Survey, Cambridge CB3 0ET, UK

S. J. Edwards
Department of Earth and Environmental Sciences, University of Greenwich, Chatham Maritime, Kent ME4 4TB, UK

I. J. Parkinson
Department of Earth Sciences, The Open University, Milton Keynes MK7 6AA, UK

Present address:
[1]Department of Earth Sciences, University of Cardiff, Cardiff CF1 3YE, UK
e-mail: PearceJA@cardiff.ac.uk

Editorial responsibility: J. Hoefs

Introduction

Peridotites from supra-subduction zone settings can provide important information on melt generation and melt–mantle interaction above subduction zones, contribute to our understanding of the original tectonic setting of formation of ophiolite complexes, and help in the understanding of crustal accretion in arc–basin systems. Few supra-subduction zone peridotites have so far been studied in the same detail as the so-called abyssal and orogenic peridotites that mainly encompass peridotites originally emplaced in ocean ridge and passive continental margin settings, respectively. Those that have are primarily from the Japan–Mariana–Philippine region, such as Ichinomegata (Takahashi 1980), the

Mariana–Bonin forearc (Bloomer 1983; Bloomer and Hawkins 1983; Ishii 1985; Ishii et al. 1992; Parkinson et al. 1992; Parkinson and Pearce 1998) and the Luzon arc (Maury et al. 1992). Here, we present for the first time the petrography, major and trace element bulk rock geochemistry, and mineral geochemistry of peridotites from the South Sandwich arc–basin system in the southernmost Atlantic. We use the results to investigate magma genesis and magma–mantle interaction in a subduction zone setting.

Geological and tectonic setting

The Scotia Sea region of the southernmost Atlantic is the product of interaction of four plates: the South American plate (SAM), the Antarctic plate (ANT), the Scotia plate (SCO) and the Sandwich plate (SAN) (Fig. 1a). SAM and ANT are major plates bounded by the slow-spreading SAM–ANT Ridge (Barker and Lawver 1988). SCO and SAN are micro-plates that largely comprise lithosphere of the arc–basin systems formed during the 30–40 Ma of eastward subduction of SAM oceanic lithosphere (Barker and Burrell 1977; Barker 1995). SCO contains oceanic lithosphere from the western flank of the presently active East Scotia Sea back-arc spreading centre together with trapped fragments of lithosphere formed during the early evolution of the subduction system. SAN is a micro-plate comprising oceanic lithosphere from the eastern flank of the East Scotia Sea spreading centre together with the presently active South Sandwich island arc and its forearc. SAN is bounded in the east by the South Sandwich Trench, which is retreating eastwards in response to rapid rollback of the subducting SAM plate (Barker 1995).

The two sets of peridotites which form the basis for this paper were recovered during dredging programmes undertaken by the British Antarctic Survey in the 1980s. One set is from the inner wall of the South Sandwich Trench (dredges 52–54) and will be termed the South Sandwich forearc peridotites. The other was dredged just south of the intersection between the South Sandwich Trench and the SAM–ANT Ridge (dredge 110) and will be termed the South Sandwich TFI (Trench–Fracture Zone intersection) peridotites.

The South Sandwich forearc peridotite locality lies at the north-eastern corner of the forearc about 100 km east of the active volcanic arc island of Zavodovski. The forearc here is narrow, probably as the result of extensive tectonic erosion (Vanneste and Larter 1997). Geosat gravity data (Fig. 1b) reveal a steep gravity gradient across the forearc and show that the mid-slope high dredged at sites 52–54 has a high positive gravity anomaly (Livermore et al. 1994). The three dredges recovered only peridotites. These are highly serpentinised but there is no evidence of any serpentinite seamounts resembling those in the Bonin–Mariana forearcs (Fryer and Pearce 1992). Most likely, extensional and erosional tectonic processes exposed the peridotites at the seafloor.

The forearc itself has no obvious magnetic lineations. However, the magnetic profile across the forearc, arc and back-arc basin (Fig. 2) reveals that the western flank of the East Scotia Sea contains anomalies up to 5 (10 Ma) and possibly 5b (15 Ma) (Barker and Hill 1981; Barker 1995). The eastern flank is cut off between anomalies 4 and 5 (ca. 8 Ma). This implies that the present arc is built on marginal basin lithosphere formed at the East Scotia Ridge. The peridotites could therefore represent tectonically exposed lithosphere formed during the early evolution of the arc–basin system. Alternatively, they could represent lithosphere accreted from the subducting South American plate or even the residue from mantle melting beneath the South Sandwich arc.

The South Sandwich TFI peridotite locality lies just south of a long transform offset of the SAM–ANT Ridge on a north-facing scarp of an ill-defined ridge in an area of complex bathymetry (Fig. 1b). The dredge recovered both peridotites and basalts. Although there are magnetic anomalies in the dredged region, these have not yet successfully been calibrated. The precise setting of the TFI peridotites is thus unclear. They may have formed at the SAM–ANT Ridge, which disappeared at that latitude during a ridge–trench collision event at about 3.2 Ma (Barker 1995). Alternatively, they may be related to a small back-arc ridge segment that developed north of the South Scotia Ridge following the ridge subduction event. The significant vesicularity and chemical composition (slightly elevated LILE/HFSE ratios) of basalts in that area indicate a small subduction zone influence (Hamilton 1989; Pearce et al., in preparation) and thus suggest that the latter option is the more likely, at least for the lavas. However, there are other, more complex settings to be considered: the peridotites could represent a piece of forearc mantle lithosphere displaced into its

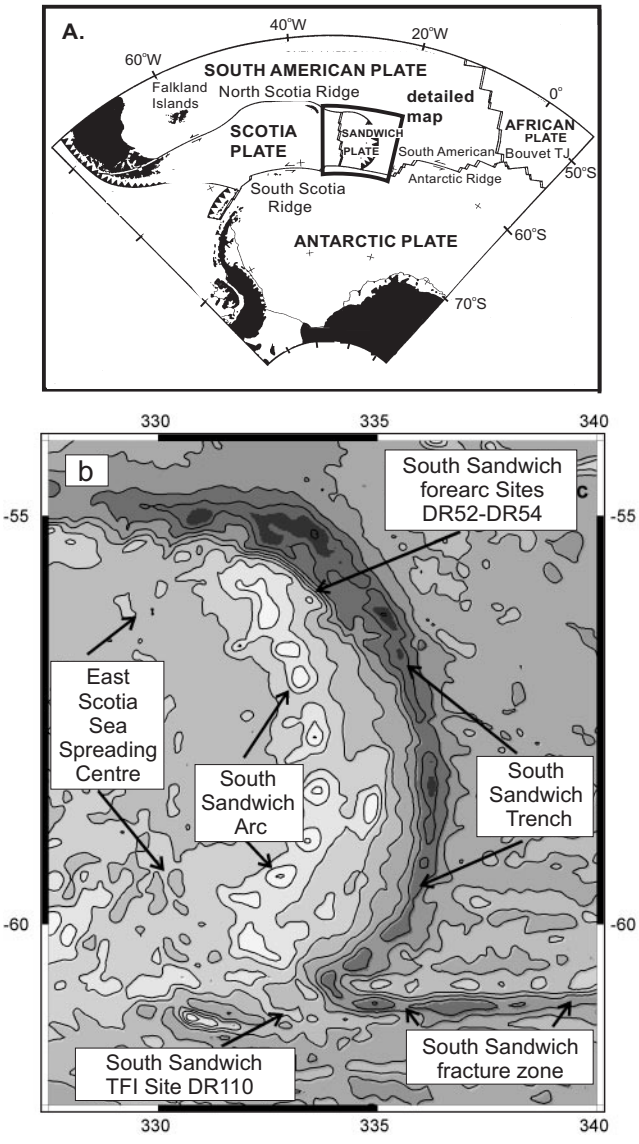

Fig. 1 **a** Regional tectonic setting of the South Sandwich arc–basin system **b** Free-air gravity map of the South Sandwich arc–basin system showing the location of the peridotites analysed in this study. Dredge sites 52–54 lie on the steep, outer slope of the mid-slope high (also a prominent slope on the gravity anomaly map). Dredge site 110 lies on a ridge oriented slightly N of W, south of the currently active transform and probably part of a transform that was active until recently. Contours are at 60-mgal intervals from a maximum of about +240 above the arc to a minimum of about −270 above the trench (see Barker 1995 for a more detailed, colour version)

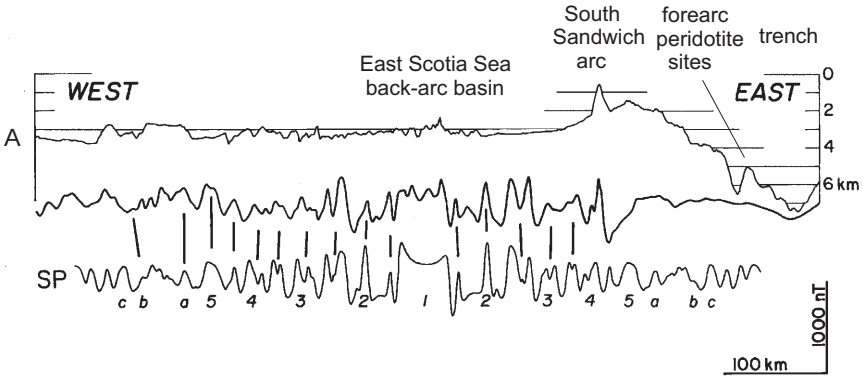

Fig. 2 West–east bathymetric, magnetic anomaly and synthetic magnetic anomaly (SP) profiles crossing the northern East Scotia Sea and South Sandwich forearc close to dredge sites 52–54 (taken from Fig. 7.10 of Barker 1995). Older magnetic lineations on the western flank of the back-arc spreading centre do not have equivalents on the eastern flank, suggesting that the upper forearc is made up of East Scotia Sea lithosphere that underwent subduction-related, tectonic disruption

present position during plate reorganisation, or mantle that 'leaked' out of the mantle wedge and fed a SAM–ANT ridge segment during the ridge–trench collision.

Analytical methods

Textural and modal analyses were undertaken following the approach of Edwards and Malpas (1996). Table 1 gives our 'best estimates' of the proportions of primary minerals in the peridotites. This was a difficult task because of the high extent of serpentinisation and oxidation. Our principal method utilised the SEM with EDAX attachment at Greenwich University to construct chemical maps of the thin sections, from which volume estimates could be made (mineral modes). In addition, we used linear programming to find the proportions by weight of the minerals that gave the best (minimum Σr^2) fit to the whole rock analysis (chemical modes). Only the immobile elements Ti, Al, Ni, V and Cr were used and the solution was constrained to positive values. For most samples, there was a good correspondence between the mineral and chemical modes. The exceptions were the highly altered harzburgites from the South Sandwich forearc where the mineral modes gave significantly higher proportions of olivine than the chemical modes. In these cases, we have used the chemical modes: otherwise the modes would give Ni contents that are too high, and Ti and Al contents that are too low, compared with the measured values. We also used the chemical modes to give a more accurate estimate of the proportion of spinel than was possible using the mineral modes. We further estimated the degree of alteration from the percentage of relict phases using the chemical maps. These results are also listed in Table 1.

Whole-rock analyses of the peridotites were carried out at Durham University. Major elements and first-order transition metals were analysed by XRF (Philips 1400). Some 30 trace elements, including the first-order transition metals, were analysed by ICP-MS (PE Elan 6000). Analysis of the low-abundance trace elements (Y, Zr, Nb, REE, Hf, Th, U) by ICP-MS adopted well-established methods (Pearce et al. 1995) but with ultra-pure acids and long count times. Detection limits lie typically between 0.01 and 0.001 ppm. Precisions for peridotite analysis (expressed as %RSD) were determined from multiple dissolutions and analyses of our Beni Bousera spinel peridotite internal standard, which is very close to a fertile MORB mantle composition. The USGS international standard peridotite, PCC1, was analysed as an independent standard. These data are given in Table 2.

Mineral phases were analysed for major and minor elements by wavelength dispersive electron microprobe on both the Camebax machine at Edinburgh University and the Cameca SX100 at the Open University. We used the PAP procedure (Pouchou and Pichoir 1985) to process the two sets of data. Particular attention was paid to the analysis of key minor elements in spinels, using long count times for Ti and V. The two data sets were within error in almost all cases with detection limits in the range of 0.01–0.03 wt% for all major elements. Average data for spinels, olivines and pyroxenes are given in Tables 3–5.

We carried out additional analyses of the spinels for ferric iron on the Open University microprobe. This was done using Wood and Virgo's (1989) standard samples 8311, 8315, 8316 and 79-1, on which ferric iron had been determined by Mössbauer spectroscopy. We determined oxygen fugacities using the methods of Nell and Wood (1991) and Ballhaus et al. (1991) based on the reaction $6Fe_2SiO_4 + O_2 = 3Fe_2Si_2O_6 + 2Fe_3O_4$ (see also Parkinson and

Table 1 Petrographic data for the South Sandwich peridotites studied in this paper. Rock types are: harzburgite (*Hz*), transitional (*Trans.*), dunite and lherzolite (*Lhz*). Mineral abbreviations are conventional. All percentages except serpentine (*serp.*) are estimated primary values. Serp. gives the percentage of alteration. *TFI* Trench–fracture zone intersection; *Porph.* porphyroclastic; *Impreg.* impregnation

Location	Sample no.	Rock type	Ol.	Opx	Cpx	Pl.	Sp.	Serp.	Petrography
Forearc	DR.52.11	Hz	75	20	4	–	0.7	75	Porph.
Forearc	DR.52.12	Hz	75	20	4	–	0.5	80	Porph.
Forearc	DR.54.10	Trans.	77	20	2	–	0.9	90	Porph./Impreg.
Forearc	DR.52.8	Trans.	86	10	3	–	1.1	>95	Porph.
Forearc	DR.52.4	Trans.	83	8	8	–	0.7	>85	Porph./Impreg.
Forearc	DR.52.5	Dunite	>95	–	<5	–	0.4	>85	Cumulate
Forearc	DR.52.6	Dunite	99	–	–	–	0.8	>85	Cumulate
Forearc	DR.53.2	Dunite	99	–	–	–	0.7	>90	Cumulate
Forearc	DR.53.3	Dunite	>95	<5	–	–	1–2	>95	Cumulate
TFI	DR.110.1	Lhz	61	18	13	7	0.6	65	Porph./Impreg.
TFI	DR.110.2	Lhz	75	16	7	1	0.9	55	Porph./Impreg.
TFI	DR.110.3	Lhz	71	15	8	5	0.9	75	Porph./Impreg.
TFI	DR.110.4	Hz	76	20	2	1–2	0.6	65	Porph.

Table 2 Geochemical analyses of peridotite samples from the South Sandwich arc–basin system (for details, see text). *n.d.* = not detected; *d.l.* detection limit; *FMM* fertile MORB mantle. Values in wt. % (oxides and LOI) and ppm (elements)

Sample (DR)	52.11	52.12	54.10	52.8	52.4	52.5	52.6	53.2	53.3	110.1	110.2	110.3	110.4	d.l.	%RSD (FMM)	PCC1
Location	Forearc	Forearc	Forearc	Forearc	Forearc	Forearc	Forearc	Forearc	Forearc	TFI	TFI	TFI	TFI			
Rock	Hz	Hz	Trans.	Trans.	Trans.	Dunite	Dunite	Dunite	Dunite	Lhz	Lhz	Lhz	Hz		–	
SiO_2	43.58	45.66	46.30	43.33	45.08	43.28	43.92	46.60	46.26	45.20	44.46	44.77	45.00	–	–	–
TiO_2	0.02	0.01	0.01	0.01	0.01	0.00	0.05	0.00	0.00	0.24	0.08	0.11	0.07	–	–	–
Al_2O_3	0.88	0.78	0.91	0.67	0.58	0.19	0.16	0.13	0.12	3.68	1.80	3.47	1.97	–	–	–
Fe_2O_3	9.36	10.07	10.34	11.14	10.84	10.63	10.60	10.28	10.27	9.06	9.10	9.32	9.02	–	–	–
MnO	0.11	0.08	0.07	0.09	0.15	0.08	0.10	0.07	0.13	0.15	0.13	0.14	0.13	–	–	–
MgO	41.23	42.74	41.31	43.61	41.53	46.54	44.42	41.36	42.29	36.21	42.48	39.75	42.21	–	–	–
CaO	4.46	1.05	0.68	1.25	1.66	0.17	0.08	0.32	0.49	4.40	2.81	2.87	1.81	–	–	–
Na_2O	0.08	0.14	0.10	0.19	0.47	0.37	0.61	0.27	0.34	0.13	0.02	0.12	0.11	–	–	–
K_2O	0.03	0.00	0.02	0.01	0.01	0.02	0.03	0.04	0.03	0.08	0.00	0.04	0.01	–	–	–
Total	*100.11*	*100.60*	*99.75*	*100.20*	*100.53*	*101.35*	*100.06*	*99.17*	*99.93*	*99.15*	*100.88*	*100.60*	*100.33*	–	–	–
LOI	8.71	9.72	11.75	10.25	11.65	9.57	11.82	12.23	12.35	5.80	8.74	8.01	8.66	–	–	–
Sc	10.6	7.4	10.1	8.6	10.9	3.8	3.9	3.9	3.7	15.3	11.1	13.6	9.9	1.0	1.65	8.3
Ti	108	63	78	78	77	16	27	8.4	13	1434	444	756	390	0.87	0.91	26
Cr	2405	2134	2845	3504	2633	1560	2850	2439	2237	2630	2413	2690	2142	8.7	0.95	2680
V	49	38	63	38	88	23	32	33	48	115	55	75	55	1.9	1.83	29.1
Ni	2059	2102	2443	2400	2541	2607	2470	2777	2589	1770	1890	1875	1882	1.0	0.70	2411
Co	99	94	98	113	117	120	121	118	109	84	100	99	104	0.04	0.52	113
Cu	23	23	23	8	60	2	5	1	6	120	14	31	14	0.06	0.56	7.7
Zn	65	41	45	48	57	30	40	45	48	32	36	36	37	1.0	2.15	36
Ga	1.01	0.72	1.01	0.83	0.83	0.19	0.41	0.18	0.48	4.92	1.71	2.91	1.84	0.13	2.02	0.58
Rb	0.38	0.26	0.61	0.33	0.12	0.24	0.23	0.41	0.70	1.51	0.27	0.79	0.33	0.02	3.78	0.065
Sr	892	700	7	13	87	6	13	26	9	48	160	18	94	0.04	0.89	0.36
Y	0.43	0.24	0.43	0.21	0.85	0.27	0.41	0.11	0.65	7.57	2.04	2.99	1.59	0.005	1.40	0.084
Zr	0.06	0.08	0.29	0.15	0.30	0.25	0.44	0.16	0.46	10.15	1.90	4.34	1.52	0.04	1.95	0.17
Nb	n.d.	n.d.	0.036	n.d.	n.d.	n.d.	0.066	n.d.	0.017	n.d.	n.d.	n.d.	n.d.	0.009	6.56	0.016
Ba	2.44	2.75	1.73	0.67	1.48	0.95	0.70	1.61	1.54	27.20	4.05	3.04	3.45	0.12	1.00	0.78
La	0.007	0.007	0.077	0.009	0.072	0.067	0.153	0.018	0.164	0.159	0.015	0.134	0.041	0.003	2.28	0.028
Ce	0.015	0.017	0.217	0.015	0.040	0.008	0.318	0.011	0.143	0.730	0.089	0.614	0.060	0.004	1.16	0.054
Pr	0.003	0.002	0.017	0.002	0.011	0.010	0.033	0.004	0.039	0.184	0.033	0.110	0.027	0.002	3.67	0.006
Nd	0.013	0.011	0.067	0.008	0.057	0.050	0.140	0.017	0.172	1.232	0.244	0.583	0.194	0.006	2.65	0.026
Sm	0.010	0.004	0.018	0.003	0.017	0.009	0.029	0.004	0.047	0.623	0.126	0.217	0.093	0.006	2.51	0.007
Eu	0.005	0.003	0.006	0.003	0.005	0.003	0.011	0.001	0.012	0.249	0.050	0.094	0.038	0.002	2.43	n.d.
Gd	0.022	0.010	0.028	0.006	0.029	0.013	0.034	0.004	0.059	0.905	0.207	0.326	0.145	0.005	2.18	0.008
Tb	0.007	0.003	0.006	0.002	0.007	0.002	0.006	0.001	0.011	0.181	0.042	0.066	0.029	0.001	2.48	n.d.
Dy	0.059	0.029	0.050	0.024	0.057	0.019	0.042	0.007	0.078	1.307	0.297	0.456	0.225	0.003	1.87	0.010
Ho	0.015	0.007	0.013	0.007	0.016	0.005	0.010	0.002	0.019	0.304	0.068	0.102	0.053	0.001	0.91	0.003
Er	0.050	0.028	0.043	0.025	0.058	0.017	0.032	0.009	0.059	0.874	0.205	0.301	0.161	0.002	1.90	0.011
Tm	0.010	0.005	0.007	0.006	0.011	0.004	0.006	0.002	0.010	0.134	0.035	0.049	0.028	0.001	1.91	0.002
Yb	0.067	0.040	0.061	0.043	0.070	0.025	0.042	0.014	0.070	0.868	0.230	0.318	0.190	0.002	1.53	0.022
Lu	0.012	0.008	0.010	0.008	0.013	0.005	0.008	0.003	0.013	0.136	0.037	0.050	0.033	0.001	3.14	0.005
Hf	n.d.	n.d.	n.d.	n.d.	n.d.	n.d.	n.d.	n.d.	n.d.	0.336	0.078	0.146	0.062	0.004	3.29	0.003
Ta	n.d.	n.d.	n.d.	n.d.	n.d.	n.d.	0.011	n.d.	n.d.	n.d.	n.d.	n.d.	n.d.	0.005	6.21	n.d.
Th	0.005	0.002	0.022	n.d.	0.005	n.d.	0.033	0.003	0.020	0.002	n.d.	0.007	n.d.	0.001	5.30	0.010
U	0.666	0.931	0.725	1.580	0.986	0.926	1.098	1.150	1.161	0.054	0.283	0.242	0.507	0.001	5.30	0.004

Table 3 Microprobe analyses of chrome spinels in peridotites from the South Sandwich forearc and trench–fracture zone intersection (TFI). See the text for analytical details. Fe_2O_3 has been determined by stoichiometry

Sample	DR.52.11	DR.52.12	DR.54.10	DR.52.8	DR.52.4	DR.52.5	DR.52.6	DR.53.3	DR.110.1	DR.110.2	DR.110.3	DR.110.4
Location	Forearc	Forearc	Forearc	Forearc	Forearc	Forearc	Forearc	Forearc	TFI	TFI	TFI	TFI
Rock	Hz	Hz	Trans.	Trans.	Trans.	Dunite	Dunite	Dunite	Lhz	Lhz	Lhz	Hz
Al_2O_3	33.50	29.44	32.76	26.44	25.29	13.94	13.75	10.74	46.95	37.07	39.61	30.19
Cr_2O_3	33.21	35.02	33.17	39.75	40.92	50.94	51.71	54.69	17.61	27.46	25.27	31.91
V_2O_3	0.25	0.25	0.22	0.21	0.29	0.18	0.18	0.27	0.19	0.18	0.17	0.31
FeO	15.14	15.72	15.69	17.27	17.73	20.32	20.10	21.54	12.37	12.83	11.91	17.84
Fe_2O_3	2.86	3.94	3.32	3.74	3.63	5.74	5.04	4.89	4.53	5.47	4.95	6.86
MgO	14.24	13.08	13.69	12.27	11.78	9.07	9.20	7.87	17.21	15.93	16.75	11.74
TiO_2	0.09	0.11	0.10	0.17	0.12	0.21	0.26	0.22	0.20	0.41	0.55	0.59
MnO	0.24	0.25	0.33	0.28	0.28	0.37	0.38	0.43	0.15	0.18	0.20	0.30
CoO	0.09	0.11	0.10	0.09	0.10	0.10	0.10	0.09	0.05	0.08	0.06	0.14
SiO_2	0.04	0.04	0.03	0.04	0.03	0.04	0.03	0.03	0.02	0.02	0.03	0.02
NiO	0.15	0.13	0.12	0.13	0.12	0.10	0.13	0.04	0.28	0.19	0.26	0.24
ZnO	0.25	0.26	0.28	0.26	0.26	0.23	0.24	0.26	0.13	0.17	0.15	0.43
Total	*100.06*	*98.35*	*99.81*	*100.65*	*100.55*	*101.24*	*101.12*	*101.07*	*99.69*	*99.99*	*99.91*	*100.57*
Mg#	0.626	0.597	0.608	0.559	0.542	0.443	0.449	0.394	0.712	0.689	0.715	0.540
Cr#	0.387	0.424	0.404	0.481	0.498	0.660	0.672	0.774	0.201	0.332	0.300	0.415
Fe#	0.032	0.046	0.037	0.043	0.042	0.071	0.062	0.062	0.047	0.059	0.053	0.078

Table 4 Microprobe analyses of olivines in peridotites from the South Sandwich forearc and trench–fracture zone intersection (TFI). See the text for analytical details

Sample	DR.52.11	DR.52.8	DR.52.4	DR.52.5	DR.52.6	DR.53.2	DR.53.3	DR.110.1	DR.110.2	DR.110.3	DR.110.4
Location	Forearc	Forearc	Forearc	Forearc	Forearc	Forearc	Forearc	TFI	TFI	TFI	TFI
Rock	Hz	Trans.	Trans.	Dunite	Dunite	Dunite	Dunite	Lhz	Lhz	Lhz	Hz
SiO_2	40.10	41.08	39.43	41.71	40.58	41.50	41.68	40.98	40.76	40.95	41.33
TiO_2	0.02	0.00	0.00	0.00	0.00	0.00	0.00	0.01	0.01	0.00	0.01
Al_2O_3	0.02	0.00	0.02	0.00	0.00	0.00	0.00	0.00	0.01	0.01	0.02
FeO	9.48	9.08	8.80	8.42	8.09	7.33	7.44	11.51	9.25	9.16	8.75
MnO	0.14	0.13	0.13	0.12	0.12	0.11	0.11	0.16	0.14	0.13	0.13
MgO	49.33	49.58	48.01	51.12	49.96	50.69	50.09	48.91	50.52	48.18	49.48
CaO	0.02	0.02	0.02	0.05	0.03	0.04	0.04	0.02	0.03	0.04	0.04
Na_2O	0.03	0.02	0.02	0.01	0.01	0.01	0.02	0.00	0.01	0.00	0.00
Cr_2O_3	0.02	0.01	0.01	0.01	0.01	0.00	0.01	0.00	0.02	0.01	0.01
NiO	0.24	0.39	0.38	0.36	0.35	0.34	0.33	0.40	0.39	0.35	0.33
Total	*99.40*	*100.31*	*96.82*	*101.80*	*99.15*	*100.02*	*99.72*	*101.99*	*101.14*	*98.83*	*100.10*
Fo	0.903	0.907	0.907	0.915	0.917	0.925	0.923	0.883	0.907	0.904	0.910
Fa	0.097	0.093	0.093	0.085	0.083	0.075	0.077	0.117	0.093	0.096	0.009

Table 5 Microprobe analyses of pyroxenes in peridotites from the South Sandwich forearc and trench–fracture zone intersection (TFI). See the text for analytical details

Sample	DR.52.11	DR.54.10	DR.52.4	DR.52.5	DR.110.1	DR.110.2	DR.110.3	DR.110.4	DR.52.11	DR.54.10	DR.52.4	DR.110.1	DR.110.2	DR.110.3	DR.110.4
Mineral	cpx	cpx	cpx	cpx	cpx	cpx	cpx	cpx	opx	opx	opx	opx	opx	opx	opx
Rock	Hz	Trans.	Trans.	Dunite	Lhz	Lhz	Lhz	Lhz	Hz	Trans.	Trans.	Lhz	Lhz	Lhz	Lhz
SiO_2	53.03	52.40	54.38	54.79	50.58	50.75	51.60	51.72	56.89	55.85	57.44	54.11	54.49	55.27	55.84
TiO_2	0.11	0.12	0.08	0.06	1.33	0.53	0.74	0.56	0.04	0.04	0.03	0.35	0.19	0.23	0.23
Al_2O_3	2.75	2.70	1.60	1.23	5.26	5.33	4.78	4.71	2.28	2.51	1.69	4.90	3.96	4.05	3.17
FeO	2.52	2.17	2.07	1.64	3.21	3.19	2.62	2.86	6.44	6.25	6.25	7.48	6.38	6.16	5.96
MnO	0.08	0.08	0.07	0.05	0.09	0.10	0.09	0.09	0.15	0.02	0.15	0.16	0.14	0.14	0.14
MgO	17.36	16.37	18.03	17.59	16.01	16.69	16.04	17.01	34.63	33.46	35.03	32.05	32.89	32.48	33.12
CaO	23.38	24.17	24.18	24.58	21.39	20.41	24.17	22.97	0.50	0.85	0.57	1.36	1.49	1.04	1.37
Na_2O	0.14	0.19	0.10	0.37	0.62	0.58	0.64	0.55	0.02	0.02	0.01	0.04	0.05	0.03	0.03
Cr_2O_3	0.96	0.96	0.57	0.81	0.86	1.18	1.05	1.24	0.45	0.59	0.39	0.54	0.71	0.66	0.65
V_2O_3	0.05	0.05	0.04	0.03	0.08	0.04	0.04	0.04	0.03	0.02	0.02	0.01	0.03	0.02	0.03
NiO	0.05	0.03	0.05	0.04	0.05	0.05	0.04	0.04	0.08	0.09	0.08	0.09	0.09	0.08	0.07
ZnO	0.00	0.00	0.00	0.00	0.00	0.02	0.02	0.01	0.01	0.00	0.01	0.00	0.00	0.00	0.02
Total	*100.43*	*99.24*	*101.17*	*101.19*	*99.48*	*98.87*	*101.83*	*101.80*	*101.52*	*99.70*	*101.67*	*101.09*	*100.42*	*100.16*	*100.63*
En	0.488	0.476	0.493	0.486	0.482	0.486	0.460	0.484	0.897	0.890	0.900	0.861	0.876	0.885	0.885
Fs	0.040	0.032	0.032	0.026	0.054	0.051	0.042	0.046	0.094	0.093	0.091	0.113	0.095	0.094	0.089
Wo	0.473	0.492	0.475	0.488	0.463	0.463	0.498	0.470	0.009	0.016	0.009	0.026	0.029	0.020	0.026

Pearce 1998). Table 6 gives the data obtained by this method. Standard errors are 0.2 to 0.3 log units for samples with chromites up to Cr# of 0.55, the upper limit of the calibration. Chromites with higher Cr# (i.e. the dunites) have higher errors because of the uncertainties over the role of vacancies in the chromite structure at these compositions.

Peridotite petrography

The two sets of peridotites encompass a wide range of mineralogies and textures. Table 1 gives our estimates of the mineral proportions and hence classifications of the samples with the caveat that these are limited by sample size and by the considerable degrees of serpentinisation and oxidation.

The South Sandwich forearc peridotites from dredge sites 52–54 fall into three groups. Samples DR.52.11 and DR.52.12 are harzburgites with similar original compositions of about 75% olivine, 20% orthopyroxene, 4% clinopyroxene and accessory chrome spinel. Their orthopyroxene porphyroclasts are deformed and typically have lobate boundaries and contain olivine inclusions. The latter may be a three-dimensional manifestation of incongruent dissolution of orthopyroxene or the result of trapping during asthenospheric recrystallisation of orthopyroxene. The spinel may also poikilitically enclose olivine (as for sample DR.54.10 in Fig. 3a).

Samples DR.52.4 and DR.52.8 have a higher proportion of olivine than the harzburgites described above, but also contain a high proportion of clinopyroxene compared to orthopyroxene. We estimate their modal compositions as 83–86% olivine, 3–8% clinopyroxene, 8–10% orthopyroxene and accessory spinel. Strictly, therefore, they range from harzburgites to lherzolites, although their compositions are quite different from the vast majority of residual mantle samples (Kelemen et al. 1992). Texturally, they exhibit features of both the harzburgites and the dunites (see below). This is most apparent in sample DR.52.8, which contains both relict orthopyroxene porphyroclasts enclosing olivine and discrete crystals of olivine rich in inclusions. The samples exhibit an impregnation texture in which clinopyroxene is typically intergranular, forming wehrlitic patches with olivine within harzburgite (Fig. 3b). In the text and figures, we term these samples 'transitional', meaning transitional between harzburgite and dunite or wehrlite. DR.54.10, which has a transitional texture but a harzburgite mode, has also been assigned to this group.

Samples DR.52.5, DR.52.6, DR.53.2 and DR.53.3 are dunites made up almost entirely of serpentinised olivine and chrome spinel, though DR.52.5 and DR.53.3 contain some accessory clinopyroxene and orthopyroxene, respectively. The olivine contains unidentified inclusions, possibly of crystallised, trapped melt, which are both randomly distributed and aligned in trails. These inclusions are particularly abundant in sample DR.52.5. The spinels can form partial chain textures (Fig. 3c).

Table 6 Ferric iron measurements and oxygen fugacity calculations for the chrome spinels in the South Sandwich forearc and trench–fracture zone intersection (TFI) peridotites. The oxygen fugacity data are quoted in log units relative to the QFM buffer. Cr numbers, re-calculated on the basis of the ferric iron measurements, are also shown

Sample	Location	Rock type	Fe^{3+}	Fe^{3+}/Fe(tot)	$\Delta Log(f_{O2})$	Cr#
DR.52.11	Forearc	Hz	0.030	0.137	0.01	0.398
DR.54.10	Forearc	Trans.	0.033	0.148	0.42	0.397
DR.52.8	Forearc	Trans.	0.047	0.194	0.59	0.486
DR.52.4	Forearc	Trans.	0.048	0.186	0.57	0.506
DR.52.5	Forearc	Dunite	0.091	0.283	1.85	0.695
DR.52.6	Forearc	Dunite	0.086	0.261	1.84	0.714
DR.53.2	Forearc	Dunite	0.077	0.249	2.21	0.766
DR.53.3	Forearc	Dunite	0.075	0.243	2.30	0.772
DR.110.1	TFI	Lhz	0.035	0.184	0.36	0.192
DR.110.2	TFI	Lhz	0.045	0.209	0.95	0.319
DR.110.3	TFI	Lhz	0.035	0.201	0.29	0.287
DR.110.4	TFI	Hz	0.069	0.264	1.26	0.416

Texturally, however, it is not possible to distinguish between a cumulate origin and an origin by melt–mantle interaction, except in sample DR.52.3, which contains deformed orthopyroxene.

The peridotites from site DR.110 are also highly serpentinised. The original mineral compositions were approximately 61–76% olivine, 15–20% orthopyroxene, 2–13% clinopyroxene, 1–7% plagioclase and accessory chrome spinel. The rocks therefore classify as lherzolites (DR.110.1–3) and harzburgite (DR.110.4). The samples typically consist of orthopyroxene and clinopyroxene porphyroclasts (2–5 mm) with exsolution lamellae and lobate grain boundaries in a matrix of smaller (0.5–3 mm) olivine crystals with lobate or straight (annealed) boundaries. This texture indicates that the rocks were the product of partial melting or reaction followed by deformation and static recrystallisation, typical of oceanic mantle tectonite. The orthopyroxene crystals are typically weakly deformed. Aggregates of smaller crystals (ca. 0.5 mm) of orthopyroxene associated with clinopyroxene and plagioclase indicates melt impregnation (Fig. 3d, e). Spinels have an amoeboid habit and are usually associated with the pyroxene aggregates (Fig. 3f).

Mineral compositions

Mineral compositions vary considerably between the dredged samples, as can be seen in Tables 3–5. They are perhaps best illustrated on the plot of the Cr# in spinel against the Fo content of olivine (Fig. 4). The South Sandwich forearc peridotite samples vary from the harzburgites (average Fo content of olivine = 0.900, average Cr# of spinel = 0.40), through the transitional samples (Fo = 0.906, Cr# = 0.51) to the dunites (Fo = 0.915, Cr# = 0.73). The South Sandwich TFI peridotites have olivines with lower Fo contents (Fo = 0.885–0.904) than the forearc peridotites and spinels with lower Cr# (0.20–0.42).

As Fig. 4 shows, all samples plot within, or on the edge of, the olivine–spinel mantle array (OSMA) of Arai (1994). All but the dunites plot in the abyssal (ocean ridge) peridotite field, although this is not diagnostic as peridotites from passive margins, oceanic arcs and marginal basins may also plot in this field. Arai (1994) argues that the OSMA is a residual peridotite array and that cumulates plot off this trend to the right. If this is the case, the dunites can be inferred not to be of cumulate origin. We re-examine this inference in subsequent sections. The high Cr# and Fo values of these dunites are consistent with a supra-subduction zone origin (see also Dick and Bullen 1984; Bonatti and Michael 1989).

Of the other minerals, orthopyroxene follows a similar trend of increasing Mg# from lherzolite through harzburgite and the harzburgite/dunite transitional rocks to dunite. In contrast, clinopyroxene exhibits a decrease in Mg#.

Bulk rock compositions

It is apparent from the high (>8 wt%) loss-on-ignition (LOI) values in Table 2 that all samples are extensively serpentinised. The precise effects of serpentinisation and subsequent alteration are, however, highly variable. Simple inspection of the data in Table 2 reveals that several samples (especially DR.52.11, DR.52.12 and DR.110.2) have the high Sr and Ca contents typical of carbonate addition. The samples have erratic and usually high abundances of elements of low ionic potential (K, Na, Rb, Ba) indicative of low-temperature alteration, and all samples have very high U/Th ratios indicative of low-temperature oxidative alteration. By contrast, high field strength elements (HFSE = Ti, Zr, Al, Y, HREE) show covariations that are consistent with igneous processes (see later figures) and no significant correlation with loss-on-ignition, both indicative of little sensitivity to alteration.

Figure 5 shows the chondrite-normalised rare earth patterns. The South Sandwich forearc harzburgites DR.52.11 and DR.52.12 resemble depleted abyssal peridotites or supra-subduction zone peridotites in that MREE–HREE profiles have positive slopes indicative of high degrees of fractional melting. LREE profiles vary from depleted to slightly enriched, consistent with some trapping of, or interaction with, melt or aqueous fluids. The forearc dunites have U-shaped REE profiles characteristic of interaction between LREE-enriched melt

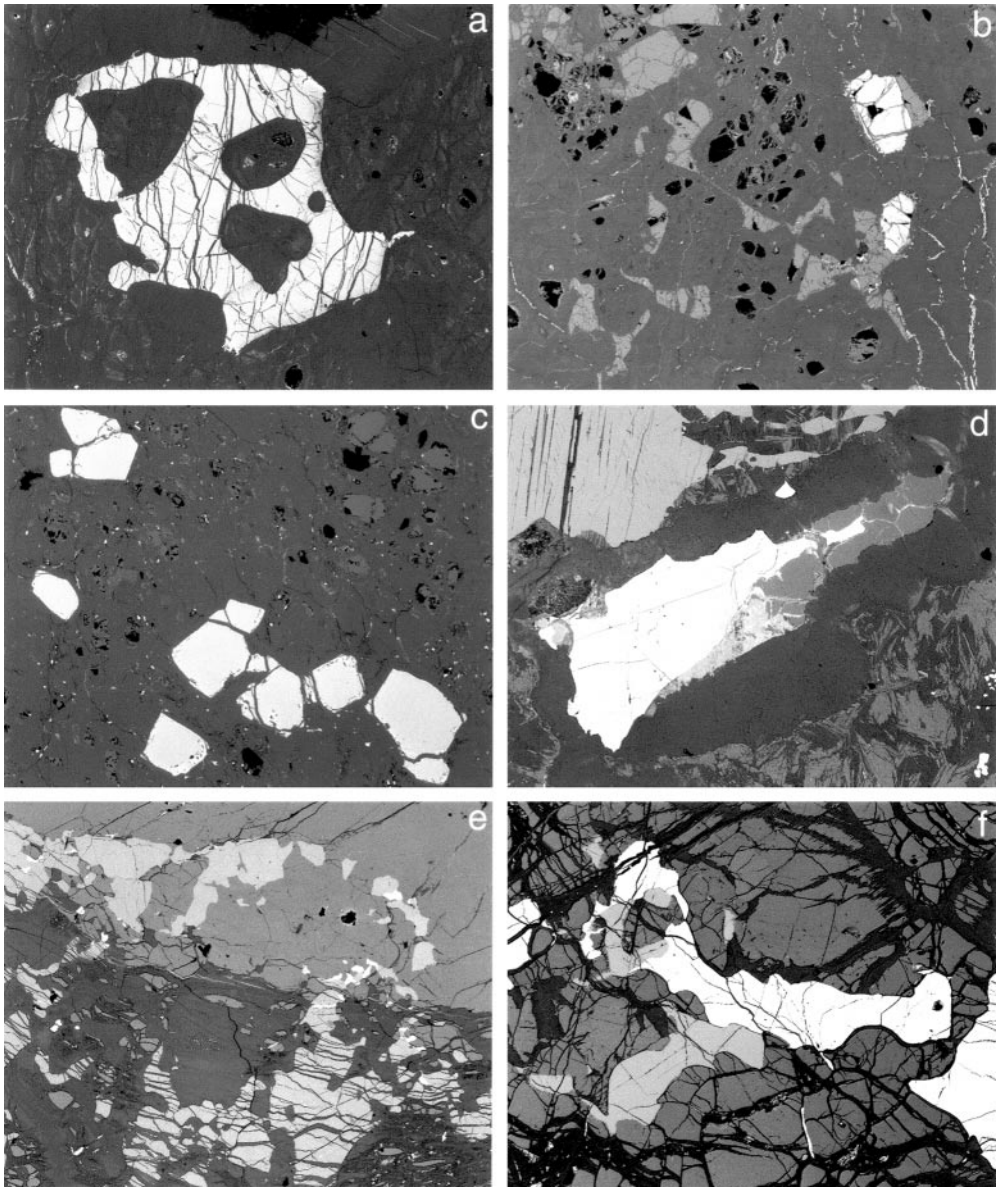

Fig. 3 Backscattered electron images from polished thin sections of peridotite samples. **a** Anhedral spinel (*white*) containing grains of serpentinised olivine in harzburgite sample DR.54.10; length of image represents 1.7 mm. **b** Blocky and delicate intragranular clinopyroxene (*light grey*) associated with spinel (*white*) in a serpentinised olivine matrix in transitional sample DR.52.4; length of image represents 2.5 mm. **c** Partial spinel chain texture (*white*) in serpentinised olivine in dunite sample DR.53.2; length of image represents 2.5 mm. **d** Altered plagioclase associated with spinel (*white*) and clinopyroxene (*light grey* in *top left*) in lherzolite sample DR.110.1; length of image represents 1.3 mm. **e** Orthopyroxene porphyroclast (*very top of image*) embayed by olivine with the contact marked by a discontinuous zone of clinopyroxene (*light grey*) and minor spinel (*white*) in lherzolite sample DR.110.2; length of image represents 1.7 mm. **f** Association of anhedral grains of clinopyroxene (*light grey*) and spinel (*white*) at an olivine–orthopyroxene contact in sample DR.110.2; length of image represents 1.3 mm

and LREE-depleted mantle residues. The transitional samples have features of both the harzburgites and the dunites: DR.52.8 has a pattern that resembles the harzburgites, whereas DR.52.4 and DR.54.10 have patterns that more closely resemble the dunites.

The South Sandwich TFI peridotites resemble fertile abyssal peridotites with generally smooth LREE-depleted patterns and flat MREE–HREE profiles. The highest abundances are in the samples with the greatest plagioclase and clinopyroxene abundances (DR.110.1 and DR110.3), i.e. the greatest degree of melt impregnation (Table 1).

An additional distinctive feature is the variable and sometimes large Ce anomalies. The contrast between the patterns for DR.110.2 (which has no anomaly) and DR.110.4 (which has a Ce anomaly but is otherwise chemically similar) suggests that these may be attributed to the mobility of La, and to a lesser extent Pr and Nd,

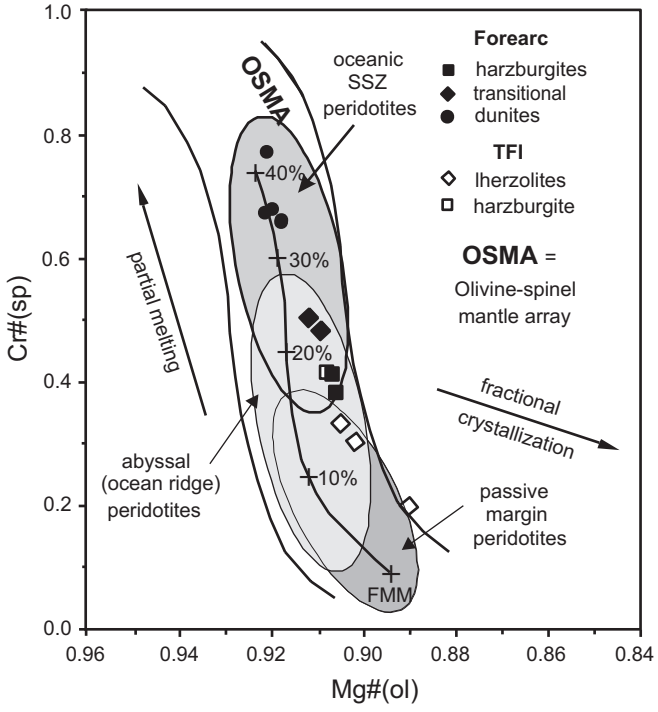

Fig. 4 Plot of spinel Cr# against olivine Mg# for the South Sandwich peridotites showing the abyssal (ocean ridge) peridotite field of Dick and Bullen (1984), the oceanic supra-subduction zone peridotite field and passive continental margin field estimated from published data, and the olivine–spinel mantle array (*OSMA*) and melting tend (annotated by % melting) of Arai (1994). *FMM* Fertile MORB mantle. The plot shows that the forearc harzburgites plot well within the abyssal peridotite field whereas the dunites plot in the oceanic subduction zone peridotite field. The TFI peridotites plot mainly in the overlap region between abyssal peridotites and passive margin peridotites

during oxidative alteration on or near the seafloor. The contrast between South Sandwich forearc dunites DR.52.5 and DR.52.6 similarly implies mobility of the trivalent LREE. If this is the case, then the Ce values may provide the best indications of the primary LREE concentrations in the peridotites, i.e. the primary LREE enrichments may be less than those indicated by the REE patterns. Note that a comparable variability in LREE was observed in the depleted peridotites from the Trinity ophiolite (Gruau et al. 1998) and attributed to secondary alteration on the basis of isotope systematics. For this reason, we use only HREE for petrogenetic modelling.

Eu anomalies are also variable but not obviously linked to alteration. Even carbonated samples with high Sr do not exhibit Eu anomalies, perhaps because Eu was mainly in the trivalent (immobile) state in the fluids during this process. The negative Eu anomalies apparent in some South Sandwich forearc dunites may be attributed to differential mobility of the light (Sm–La) and middle (Eu–Tb) REE during alteration rather to any primary process. The positive anomaly in the transitional harzburgite (DR.52.8) has no obvious explanation.

It is also apparent from the concentrations of the least mobile elements that the peridotites vary considerably in fertility. The high TiO_2 and Al_2O_3 concentrations in the Scotia TFI peridotites indicate that these are fertile peridotites, whereas the low values in the South Sandwich forearc harzburgites indicate that these are strongly depleted. Similarly, incompatible, immobile trace elements such as Zr and Y have significantly higher concentrations in the South Sandwich TFI peridotites.

Petrogenesis

Petrogenetic evolution

The petrography provides clear evidence that both sets of peridotite samples had a multi-process history. The porphyroclastic textures are consistent with an origin of at least some samples as residual mantle that has undergone high-temperature deformation at a ridge-crest or other tectonically active region. The South Sandwich forearc transitional samples and the TFI samples all show evidence for melt impregnation. The South Sandwich forearc transitional samples and some of the dunites provide additional evidence for reactions between melt and mantle. The problem is in separating and individually interpreting these different processes.

The diagram (Fig. 6a) of Cr# versus TiO_2 (spinels) is particularly effective in distinguishing between partial melting and melt–rock interaction (e.g. Arai 1992; Zhou et al. 1996). The two sets of peridotites form separate, but subparallel and positive, trends on this plot. A typical partial melting trend has been superimposed on the diagram to assist the interpretation. To construct this trend, we used published experimental data to estimate the degree of melting needed to give a particular Cr# to the spinel in the mantle residue (see also Fig. 4). We then modelled the compositions of Ti in spinels resulting from given amounts of fractional melting using an adaptation of the equation originally derived for clinopyroxene by Johnson et al. (1990), namely:

$$C_{\mathrm{ti}}^{\mathrm{sp}} = C_{\mathrm{Ti}}^{\mathrm{o}}\left(1-\frac{PF}{D_{\mathrm{Ti}}^{\mathrm{o}}}\right)^{\frac{1}{P}}\left(\frac{D_{\mathrm{Ti}}^{\mathrm{sp/l}}}{D_{\mathrm{o}}^{\mathrm{Ti}}-PF}\right)$$

where P = initial bulk solid/liquid distribution coefficient for the phases entering the melt; D^{o} = initial bulk solid/melt distribution coefficent; $D^{\mathrm{sp/l}}$ = partition coefficient between spinel and liquid; and F = degree of partial melting.

The trend drawn in Fig. 6 uses the values listed in Table 7 to model the melting of a fertile MORB mantle (FMM) with 0.18 wt% TiO_2. It represents the melting of the four-phase assemblage of olivine–clinopyroxene–orthopyroxene–spinel up to the point of clinopyroxene disappearance, then the melting of the three-phase assemblage of olivine–orthopyroxene–spinel up to the point of orthopyroxene disappearance. The final stage, the melting of the olivine–spinel assemblage, was not

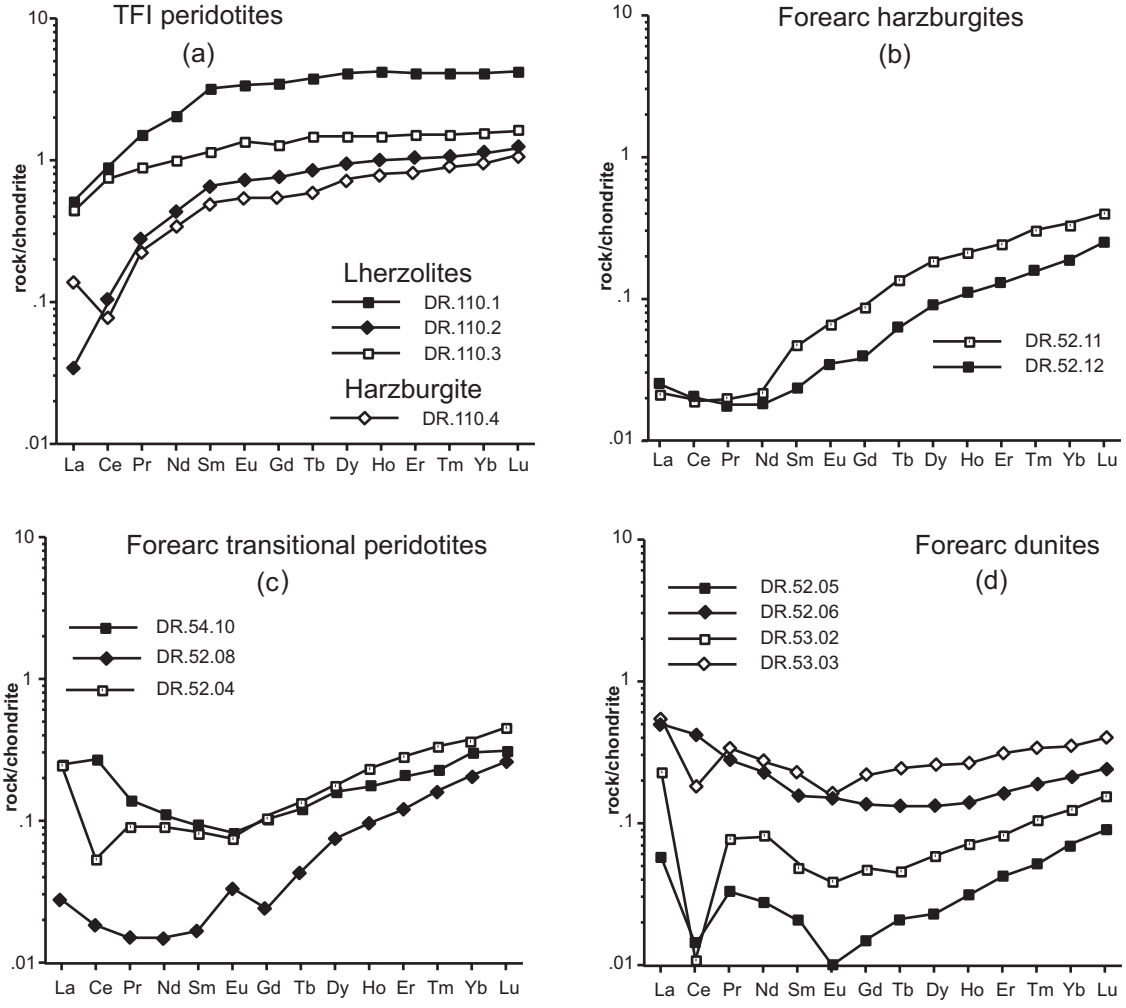

Fig. 5 Chondrite-normalised REE patterns for the South Sandwich **a** TFI and **b–d** forearc peridotites

modelled in detail. Two extreme sets of parameters were used: the congruent melting parameters of Johnson et al. (1990) and the incongruent melting parameters (and high orthopyroxene contents) of Niu (1997). The two sets of parameters were also run for varying porosities in which a small amount of melt is trapped before extraction. This was done using the equation above but treating the trapped melt as an additional phase with a proportion equal to the porosity and a partition coefficient of 1.

On the particular projection used in Fig. 6a, the melting models give very similar partial melting curves in which the Ti content of spinels rapidly decreases as the degree of melting increases and Cr# increases. The principal difference between the Johnson et al. (1990) and Niu (1997) models is that clinopyroxene disappears at about 22 and 28% melting, respectively. This causes Ti to be preferentially retained in the residue from melting of the latter model, but the difference is small. Similarly, including porosities causes retention of Ti in the melt residue, but does not change the trend significantly unless the porosity is unrealistically high ($>5\%$).

It is thus apparent that both the South Sandwich forearc and TFI peridotites form trends from low Cr#, low Ti compositions, which lie close to the melting curve, to relatively high Cr#, high Ti compositions, which are displaced significantly from the melting curve. Thus, the extrapolation of these trends back to the melting curve should give an intercept that approximates to the composition of the residual mantle that has reacted with the melt. In the case of the TFI peridotites, this intersection indicates that the residual mantle is the product of a low degree of partial melting ($<10\%$). In the case of the forearc harzburgites, the trend intersection indicates that the residual mantle was the product of 15–20% partial melting. The trends to higher Ti must then be a consequence of melt–mantle interaction through reaction or melt impregnation (Kelemen et al. 1995; Edwards and Malpas 1996; Edwards et al. 1996). Thus, for example, we can infer that forearc harzburgite DR.52.11, which lies quite close to the residual mantle composition, has undergone relatively little reaction with melt.

The simplest explanation of the reaction trends, and the one that best fits many of the textures in Fig. 3 (cf.

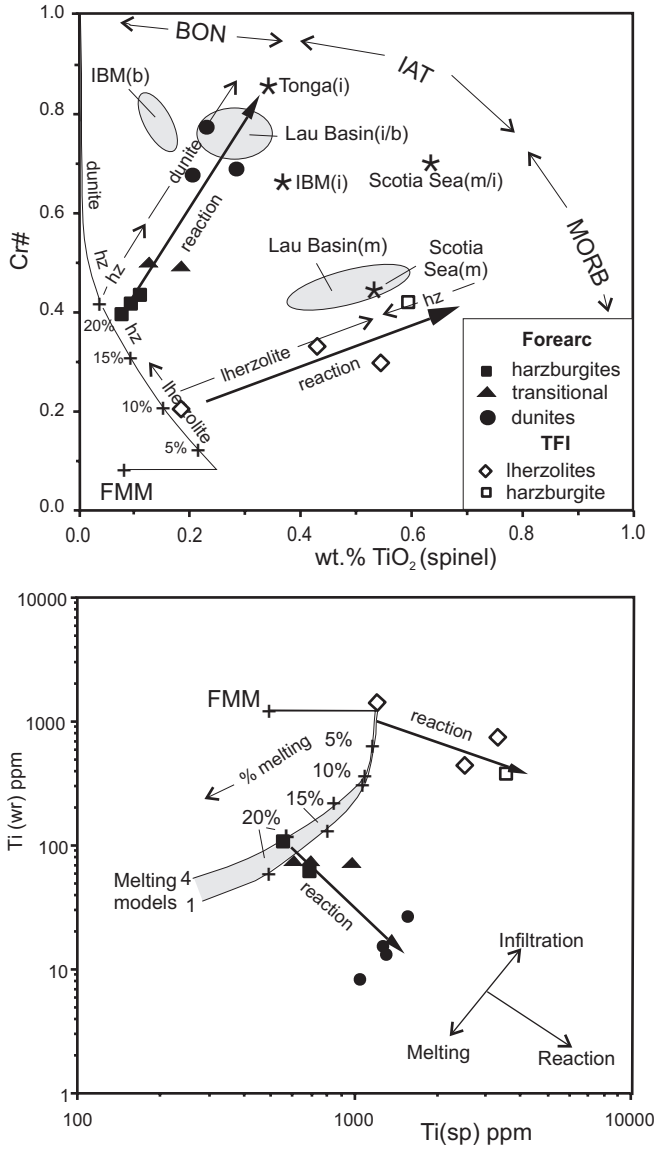

Fig. 6 **a** Plot of Cr# against TiO_2 for chrome spinel and **b** plot of chrome spinel Ti against whole rock Ti The diagrams discriminate between partial melting trends (modelled by the method described in the text and annotated according to degree of melting) and melt–mantle interaction trends (drawn empirically from the South Sandwich peridotite data). **a** shows that the Scotia TFI peridotites originated by interaction between MORB-like melt and a mantle that had experienced relatively little (< 10%) partial melting, whereas the Scotia forearc peridotites originated by interaction between a supra-subduction zone melt and a mantle that had experienced a significant (15–20%) degree of partial melting. Subscripts *m*, *i* and *b* refer to the MORB, island arc tholeiite and boninite chemistries, respectively, of the arc–basin lava spinel reference data. **b** shows that both interaction trends are marked by an increase in spinel Ti yet a decrease in whole rock Ti, indicating that reaction (i.e. dissolution of pyroxene) as well as impregnation took place. Melting *model 1* is that of Johnson et al. (1990) with zero porosity and *model 4* is that of Niu (1997) with a porosity of 1%. *Model 2*, that of Johnson et al. (1990) with 1% porosity and *model 3*, that of Niu (1997) with zero porosity, lie in the intermediate (*shaded*) region

Table 7 Values used for modelling of melting processes. The expression for the partition coefficient for spinel is an approximate fit to experimental data and reflects the strong composition dependence of this value. *F* melt fraction by wt

Phase	Johnson et al. (1990)		Niu (1997)		$K_d(Ti)_{\alpha/l}$
	X_α	p_α	X_α	p_α	
Olivine	0.57	0.10	0.52	−0.17	0.01
Orthopyroxene	0.26	0.20	0.34	0.65	0.11
Clinopyroxene	0.15	0.68	0.14	0.47	0.35
Spinel	0.02	0.02	0.02	0.05	0.1 + 1.6F

Edwards and Malpas 1996), is that the spinels have equilibrated with the interacting melt. This melt must be more Ti-rich than the last instantaneous melt extracted from the residual mantle, having pooled with earlier melt fractions and evolved by fractional crystallisation. In consequence, the spinels are more Ti-rich than those in the host peridotite and are displaced to the right of the melting trend. This explanation is supported by the compositions of spinels from some typical primitive MORB, island arc tholeiites (IAT) and boninites (BON), which predominantly plot to the right of the melting trend on the plot of Cr# against TiO_2 (spinel) (see the compilation by Arai 1992).

The examples plotted in Fig. 6a include spinels from two East Scotia Sea basalts, one containing a significant subduction component and the other with a near-MORB composition (Saunders and Tarney 1979). In the absence of spinels from South Sandwich arc basalts, we have also plotted published data on spinels from MORB, island arc tholeiites from the Lau–Tonga system (Allan 1994; Sobolev and Danyushevsky 1994) and island arc tholeiites and boninites from the Izu–Bonin–Mariana system (van der Laan et al. 1992).

It is apparent that the two South Sandwich peridotite interaction trends on Fig. 6a point to different melt end members. The end member for the forearc peridotite trend must lie close to the dunite sample with the highest Cr# (0.77), which in turn lies close (in spinel space) to depleted arc basalts, some transitional to boninites, such as those from the Lau Basin. We can thus best explain this trend by interaction between a harzburgite residual mantle and magma of depleted island arc tholeiite composition. The TFI end member lies (in spinel space) close to the MORB sample from the East Scotia Sea. We can best explain this trend by interaction between relatively undepleted abyssal peridotite (fertile MORB mantle should have spinels with about 0.08 wt% TiO_2 before reaction rising immediately to 0.18 wt% TiO_2 with equilibration during melting) and magma of MORB or transitional MORB–IAT composition.

Figure 6a, however, merely indicates that interaction has taken place, but does not indicate the type of interaction, i.e. reaction or impregnation. The plot of Ti in spinel (Ti_{sp}) versus Ti in the whole (bulk) rock (Ti_{wr}) may help to distinguish between these two processes

(Fig. 6b). This diagram demonstrates that, whereas mantle–melt interaction causes Ti_{sp} to increase within each peridotite suite, as shown on Fig. 6a, it also causes Ti_{wr} to decrease. If impregnation were the only process operating, then Ti_{wr} should increase according to the amount of melt addition because the percolating magma is richer in Ti than the host residue. The fact that Ti_{wr} decreases with the amount of interaction indicates that the infiltrating melt is also dissolving the Ti-rich phases, particularly clinopyroxene. Ti_{sp} therefore reflects the high Ti content of the infiltrating melt, whereas Ti_{wr} reflects the reaction between this melt and the host. It is likely, therefore, that reaction is an important process in both South Sandwich forearc and TFI peridotites.

Melt–mantle interaction

Because these are dredge samples with no precise geological context, there are insufficient constraints for full quantitative modelling of melt–mantle interaction. However, some semi-quantitative interpretations can be made from the geochemical data. This has been done in Fig. 7 by plotting four elements of different compatibilities (Sc which is slightly incompatible, Al which is moderately incompatible, Ti which is highly incompatible and Zr which is very highly incompatible) against the highly compatible element, Ni. Ni is a measure of both degree of melting and degree of reaction, as both parameters involve an increase in olivine content of the mantle residue.

Partial melting trends have been plotted on all four diagrams using the melting parameters of Table 7 with the partition coefficients of Pearce and Parkinson (1993) and the standard equation for fractional mantle melting. These melting trends correspond to the congruent (1) and incongruent (2) melting reactions which, for the major phases, take the form:

$$\text{olivine} + \text{orthopyroxene} + \text{clinopyroxene} = \text{melt} \quad (1)$$

$$\text{orthopyroxene} + \text{clinopyroxene} = \text{olivine} + \text{melt} \quad (2)$$

As with Fig. 6a, the TFI lherzolite and forearc harzburgites can be explained in terms of < 5 and 15–20% melting, respectively. The diagrams do, however, also highlight and discriminate between the several different types of subsequent interaction. The first is an enrichment in Ni coupled with a depletion in elements that partition into pyroxene, namely Sc, Al and Ti. Samples following this trend have high olivine:pyroxene ratios in Table 1 and can thus be interpreted as the product of pyroxene dissolution and olivine crystallisation during melt–mantle interaction, i.e. of reactions between mantle and melt saturated only in olivine. These take the form for reaction with lherzolite or clinopyroxene-bearing harzburgite and with clinopyroxene-free harzburgite, respectively:

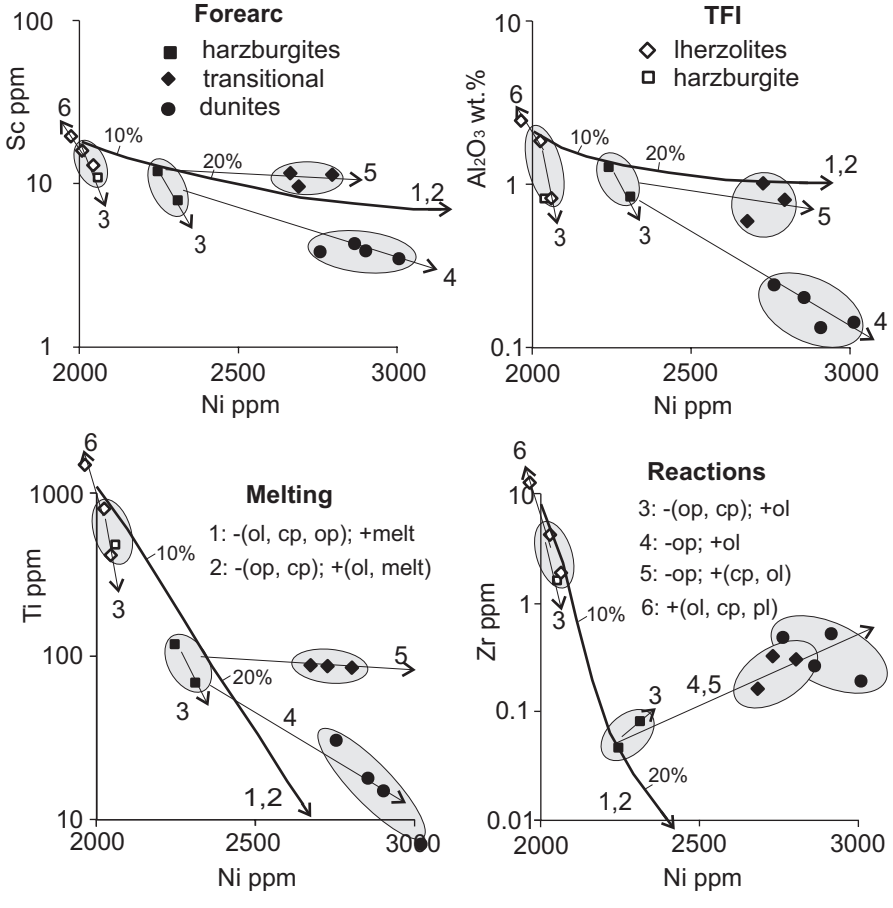

Fig. 7 Plots of Sc, Al, Ti and Zr against Ni for Scotia peridotites with partial melting trends (average of *1* and *2* calculated from the parameters in Table 7) for reference. The plot highlights the different types of melt–mantle interaction (*3–6*). Interaction with melt saturated in olivine and clinopyroxene (*5*) leads to near-constant values of Sc, Al and Ti, whereas interaction with melt saturated in olivine only (*4*) leads to depletion in these three elements. However, both types of interaction lead to an increase in the most incompatible element, Zr. In almost all cases, the partial melting and interaction trends are quite distinct. The *numbers* refer to the various reactions described in the text

$$\text{orthopyroxene} + \text{clinopyroxene} + \text{melt}_1 = \text{olivine} + \text{melt}_2 \quad (3)$$

$$\text{orthopyroxene} + \text{melt}_1 = \text{olivine} + \text{melt}_2 \quad (4)$$

Samples with both high olivine:pyroxene and high clinopyroxene:orthopyroxene ratios are also enriched in Ni. However, this is accompanied by little or no depletion in Sc, Al or Ti, the elements with relatively high clinopyroxene/liquid partition coefficients. These samples can thus be interpreted as the product of orthopyroxene dissolution and clinopyroxene and olivine crystallisation during melt–mantle interaction, i.e. of reaction between mantle and melt saturated in olivine + clinopyroxene (reaction 5). Comparable equations can be written for reactions with melt saturated in orthopyroxene, but these are not obviously relevant here.

$$\text{orthopyroxene} + \text{melt}_1 = \text{olivine} + \text{clinopyroxene} + \text{melt}_2 \quad (5)$$

Note that the most highly incompatible element plotted, Zr, follows a trend of depletion in the TFI peridotites that reflects pyroxene dissolution (reaction 3). However, it follows a trend of enrichment in the forearc peridotites regardless of the type of interaction that has taken place (reactions 4, 5 or 6). This is probably because the Zr abundances of the residual harzburgites from that setting are so low that any melt trapping or minor phase precipitation will increase the abundances of that element. Bodinier et al. (1996) have pointed out that the most highly incompatible elements can be concentrated on grain boundaries in peridotites. This may be the case here. Alternatively, the elements may be concentrated in the many inclusions within the olivines of the reaction products.

Impregnation is also apparent in some samples, notably the most plagioclase-rich of the DR.110 samples, in which the reaction is of the form:

$$\text{melt}_1 = \text{olivine} + \text{clinopyroxene} + \text{plagioclase} + \text{melt}_2 \quad (6)$$

Comparable reactions may take place in the dunites for precipitation of olivine and/or pyroxene but these cannot be positively identified.

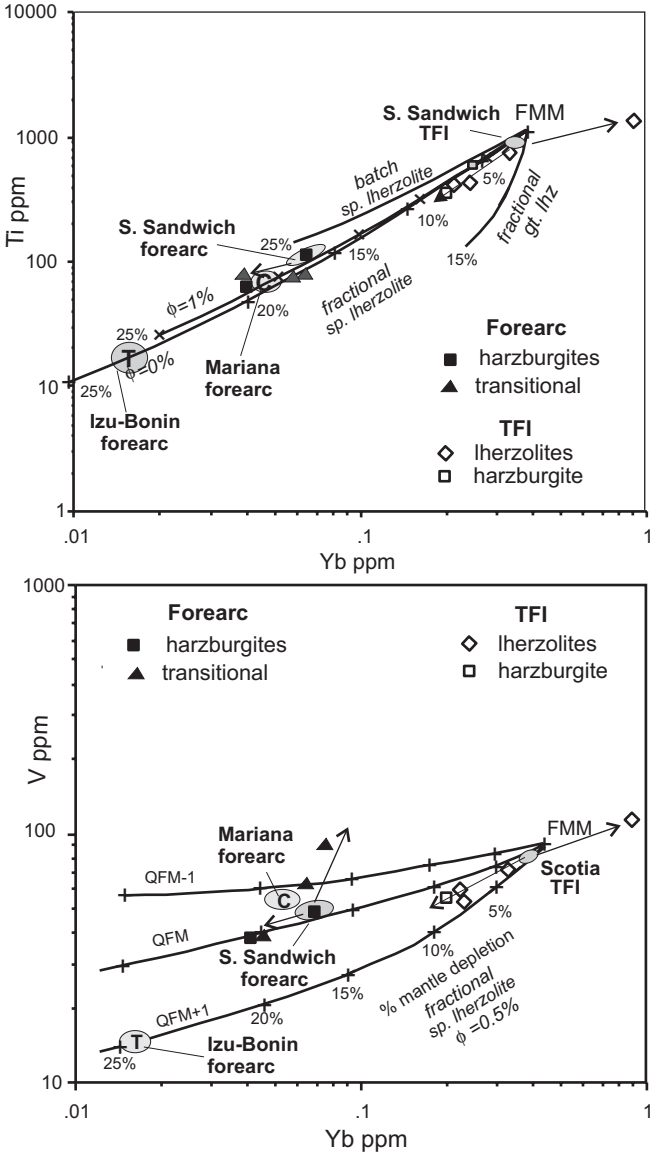

Fig. 8 Modelling of degrees of melting and oxygen fugacities using Ti–Yb and V–Yb covariations in mantle peridotites from the Scotia arc–basin system with fields for harzburgites from the Izu–Bonin–Mariana (IBM) forearcs shown for comparison. Partial melting trends use the parameters of Table 7 and the partition coefficients of Parkinson and Pearce (1998). The V data suggest that the least interacted South Sandwich forearc peridotites formed from 15–20% near-fractional melting of spinel lherzolite under QFM oxygen fugacity conditions

Nature and degree of partial melting

The nature and degree of partial melting have been quantified using the Ti–Yb plot in Fig. 8a. On this diagram, we compare the observed compositions of the least reacted samples with the theoretical batch and fractional melting trends for melting of garnet and spinel peridotites with and without a small amount of melt retention during melting (Pearce and Parkinson 1993).

Of the South Sandwich forearc peridotites, the least reacted samples (according to Fig. 6) are the harzburgites DR.52.11 and DR.52.12. The more residual of these lies on the spinel–lherzolite melting curve at a value of 17% melting, although the precise value depends on the choice of melting model, partition coefficients and degree of melt retention. This value is consistent within error of the degree of melting expected for uppermost mantle lithosphere formed by decompression melting at a centre of a mid-ocean ridge segment. It does not, however, by itself rule out an origin as lithosphere of sub-arc or marginal basin provenance, both of which may be the residues from 15–20% melting.

The South Sandwich TFI peridotite data also have to be viewed in the light of Fig. 6b. The closest to the melting trend (i.e. the least interacted) sample on that plot is DR.110.1, the other samples following a reaction trend in which Ti is lost from the sample. However, even

sample DR.110.1 has Yb greater than fertile MORB mantle (FMM) indicating some element addition (probably through melt infiltration and clinopyroxene–plagioclase crystallisation as described earlier). The likely mantle residue is therefore a lherzolite, which has experienced less than 10% partial melting before interacting with percolating MORB or transitional MORB–IAT magma.

Oxygen fugacity

Figure 9 shows the plot of $\Delta\log fO_2$(QFM) against Cr# for the South Sandwich peridotites, where $\Delta\log fO_2$(QFM) refers to the deviation from the QFM buffer expressed in log units. The fields of abyssal (mid-ocean ridge) peridotites, continental (orogenic) peridotites and oceanic arc peridotites are taken from Parkinson and Pearce (1998) and Parkinson and Arculus (1999). The reference data from the Izu–Bonin and Mariana forearcs are from Parkinson and Pearce (1998).

Both sets of South Sandwich peridotites form diagonal trends on this diagram. The forearc peridotites form a trend from the upper end of the abyssal peridotite field (the harzburgites) to the oceanic arc field (the dunites). In this, they resemble the Mariana forearc peridotites from Conical Seamount, although they are displaced to lower Cr# and/or higher oxygen fugacity.

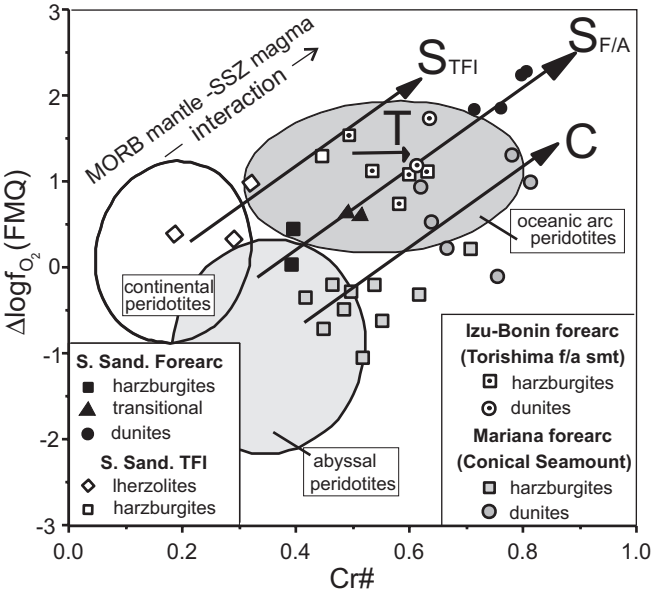

Fig. 9 Plot of $\Delta\log fO_2$(QFM) against Cr# of spinel for South Sandwich peridotite samples. The approximate fields for abyssal (mid-ocean ridge) peridotites, arc peridotites and continental (margin) peridotites are shown for reference together with peridotite data from Conical Seamount (*C*) in the Mariana forearc and Torishima Forearc Seamount (*T*) in the Izu–Bonin forearc. The plots shows that interaction trends involve increases in both oxygen fugacity and Cr# of spinel. The data are consistent with the formation of the South Sandwich peridotites (S_{TFI} and $S_{F/A}$) by interaction between lithospheric mantle protoliths of ocean ridge or transitional character and supra-subduction zone magma

As with Conical Seamount, therefore, the South Sandwich forearc peridotites can be interpreted in terms of interaction between mid-ocean ridge or back-arc mantle residues with low oxygen fugacity (represented by the harzburgites) and moderate Cr#, and island arc magma with high oxygen fugacity and high Cr# (represented by the dunites). In this model, the transitional peridotites represent intermediate products of interaction. The displacement to higher Cr# than the Mariana forearc samples may reflect the different island arc magma end members: boninite in the Mariana setting and tholeiite in the South Sandwich setting.

Note that the diagonal trends are not characteristic of all forearc peridotites. Those from Torishima Forearc Seamount in the Izu–Bonin forearc form a cluster entirely within the arc field and can be inferred as originating entirely within a single supra-subduction zone setting.

The South Sandwich TFI peridotites also form a trend towards high Cr# and high oxygen fugacities, though displaced to lower Cr# than the South Sandwich or Mariana forearc peridotites. At its lower end, the trend would extrapolate to a peridotite close to FMM in composition. Its high oxygen fugacity end member must lie at the low Cr# end of the island arc peridotite field. Although continental (orogenic) peridotites can also exhibit high oxygen fugacity as a result of melt–mantle interaction, they do not usually have such high Cr#. We therefore interpret these peridotites in terms of interaction between near-fertile mantle and a supra-subduction zone melt.

A V–Yb plot (Fig. 8b) can be used to estimate oxygen fugacities and hence better discriminate between a ridge and sub-arc genesis for the harzburgites. If oxygen fugacities are low, V (dominated by V^{III}) has high mineral–melt partition coefficients and is thus less rapidly depleted during melting than when fugacities are high and partition coefficients are low. Thus, supra-subduction zone melts, which have high oxygen fugacities, should have high V contents and their mantle residues should have correspondingly low ratios (Pearce and Parkinson 1993).

In Fig. 8b, the South Sandwich forearc peridotites form two melt–mantle interaction trends, one (with olivine as the product) towards low V and Yb and one (with olivine and clinopyroxene as the product) towards higher V and Yb. The least reacted harzburgites plot close to the QFM melting curve. This is consistent with the direct oxygen fugacity studies carried out here and thus with a pre-reaction origin at a mid-ocean ridge or a back-arc ridge with a small subduction component.

The TFI lherzolites give high oxygen fugacities (between QFM and QFM + 1) for the samples that have experienced depletion of Ti and Yb during melt–magma interaction. No samples represent true melt residua, sample DR.110.1 having experienced net impregnation, whereas the other samples have experienced extensive reaction. The intersection of the two interaction trends is consistent with the interpretations already reached, of a

slightly depleted or undepleted mantle and an oxygen fugacity close to QFM.

For comparison, our estimate (C) of the pre-interaction composition of the harzburgites from Conical Seamount implies a more reduced melting regime, between QFM and QFM–1. The equivalent estimate (T) for the Torishima Forearc Seamount gives a more oxidising regime, close to QFM + 1. These results are again consistent with the direct oxygen fugacity studies and further emphasise the presence of a spectrum of types of mantle in forearc settings: MORB lithosphere interacting with arc magma (Mariana forearc), transitional lithosphere interacting with arc magma (South Sandwich forearc); slightly depleted mantle interacting with back-arc basin magma (South Sandwich TFI); and arc lithosphere interacting with arc magma (Izu–Bonin forearc).

Tectonic implications

The results of this study reaffirm the complexities in peridotite geochemistry that are possible in the forearc tectonic setting (Parkinson and Pearce 1998). In particular, they demonstrate the possibility of peridotite formation by interaction between arc magma and pre-existing oceanic lithosphere. Figure 10 summarises the likely processes that contribute to the origin of the peridotites from the South Sandwich forearc (dredge sites 52–54). These are: (1) the original formation as the shallow residue from melting at a young East Scotia Sea (transitional MORB–IAT) spreading centre; (2) the interaction of this mantle with magmas from a young South Sandwich arc; and (3) the exposure at the seafloor through intense tectonic erosion and extension.

For the South Sandwich forearc peridotites, the oceanic lithosphere end member (Fig. 10a) was shown to be the product of 15–20% melting (Fig. 8). This is consistent with shallow residual mantle from normal ridge processes, although also with ridges near hot-spots or above subduction zones. The oxygen fugacity of this end member is, however, at the upper end of the ocean ridge range (at QFM) which may indicate that the ridge occupied a back-arc setting with a slight supra-subduction zone character (and hence augmented water content and oxygen fugacity).

An origin as East Scotia Sea lithosphere rather than SAM plate lithosphere or Central Scotia Sea lithosphere is favoured by the evidence from magnetic anomalies that the South Sandwich arc was built on pre-existing East Scotia Sea lithosphere that should also have extended into the present forearc (Fig. 2). A further point of interest is that the Scotia Sea lithosphere would have been young (ca. 5 Ma old) when the arc magmatism began. Calculations using the cooling equation (with $\kappa = 1$ mm s^{-1}; T_m–$T_s = 1300$ K) show that, by this time, sub-Moho mantle at 10 km depth below the seafloor might have cooled by only some 60 °C and thus still have been hot during the melt–mantle interaction. By contrast, any SAM plate lithosphere trapped in this position

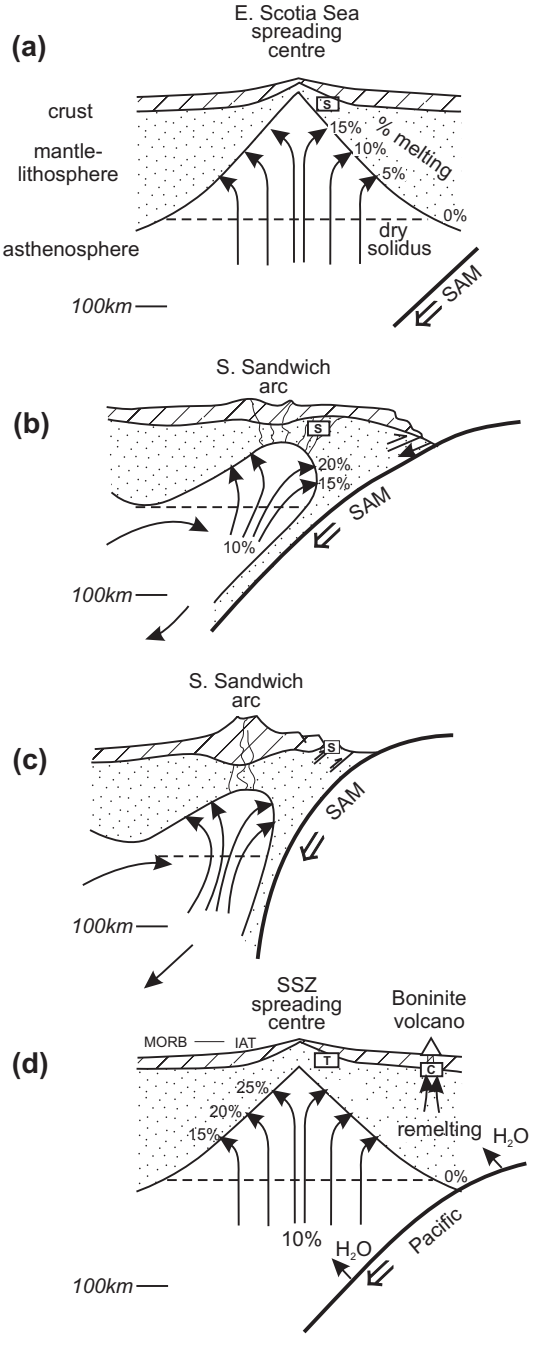

Fig. 10 Schematic diagram showing the formation of Scotia forearc peridotites by a two-stage process of **a** melting at an ocean ridge (probably an early East Scotia Sea spreading centre) followed by **b** interaction with primitive arc magma linked to the start of formation of the South Sandwich arc. Subsequent **c** tectonic thinning of the forearc then exposed the peridotites at the surface. **d** illustrates the likely setting for the Izu–Bonin–Mariana (IBM) forearc peridotites, in which melting of subduction-modified asthenosphere produces both magma and mantle lithosphere of clear supra-subduction zone character (*T* Torishima Forearc Seamount) while hydrous remelting of pre-subduction lithosphere produces boninitic magma that must rise through, and react with, overlying ocean ridge mantle (*C* Conical Seamount)

(probably about 100 Ma at the time of subduction initiation) must have been considerably colder at this depth (some 500–400 °C). Central Scotia Sea mantle lithosphere at 10 km depth (10–15 Ma at the time of arc magmatism) would have cooled to 1050–9500 °C. The inference from magnetic anomalies is thus supported by the fact that only the hot East Scotia Sea mantle lithosphere is likely to have permitted the extensive interaction without fractionation that is apparent in Fig. 4.

The interacting melt end member is, however, of clear arc character. The oxygen fugacity of the magma producing the dunites is, at QFM + 2, well within the arc range and too high for MORB. Similarly, the chrome spinels in the dunites have the high Cr# characteristic of supra-subduction zone settings. The fact that the magma became saturated in clinopyroxene before plagioclase is also more characteristic of the subduction zone than MORB settings. In this model, pre-existing mantle lithosphere interacts with magma saturated in olivine or olivine + clinopyroxene. The former type of interaction is most complete, yielding dunites with > 90% olivine. The latter is less complete, yielding harzburgites transitional to dunites or wehrlites.

The South Sandwich forearc peridotite samples resemble to a first approximation the Mariana forearc (Conical Seamount) peridotites. There are, however, differences that can best be seen in Fig. 9. The oceanic lithosphere end member of the Mariana forearc peridotites has a lower oxygen fugacity more typical of normal oceanic lithosphere. In addition, the subduction zone magma end member has higher Cr# and is probably more boninitic. Thus, the Mariana forearc peridotites probably formed by interaction between (1) MORB-like West Philippine Basin or Pacific lithosphere and (2) boninitic magma associated with subduction initiation (Fig. 10d). In contrast, the South Sandwich forearc peridotites probably formed by interaction between (1) transitional (MORB to island arc tholeiite) East Scotia Sea lithosphere and (2) island arc tholeiites typical of the South Sandwich arc (Fig. 10a, b). This difference in end members may thus reflect the difference between the nature of subduction initiation in the two forearcs.

In detail, the initiation of the IBM arc is believed to have taken place at a transform on the West Philippine Sea Ridge (e.g. Hussong and Uyeda 1981). Before subduction, therefore, the lithosphere in the Western Pacific would have had a mid-ocean ridge provenance and the mantle an 'abyssal peridotite' composition. In places, subduction caused remelting of these abyssal peridotites under hydrous conditions to produce boninitic magma. Reaction between the abyssal peridotites and boninite magma would then produce mantle of Conical Seamount type (C in Fig. 10d). Elsewhere, subduction would lead to melting of asthenosphere to produce new lithosphere of island arc tholeiite provenance. The peridotites so formed would record interaction between magma and mantle residue with the same island arc tholeiite provenance to give mantle of Torishima Forearc Seamount type (T in Fig. 10d) (Parkinson and Pearce 1998).

The South Sandwich TFI peridotites are more enigmatic, but also appear to have formed by interaction between subduction-related magma and pre-existing oceanic lithosphere. In this case, our data show that the oceanic lithosphere end member was the residue from, at most, a very small degree of melting. This is consistent with its location close to a slow-spreading SAM–ANT ridge-transform intersection. The interacting melt had a high oxygen fugacity (> QFM + 1) but a Cr# less than expected for an arc setting. It is thus possible that this interacting melt was transitional between MORB and IAT, similar to the lavas dredged from the vicinity of back-arc basin ridge segment E10 at the southernmost end of the East Scotia Sea back-arc basin. The latter developed after a ridge–trench collision dated at about 3 Ma. The most likely explanation thus involves interaction between (1) a relatively undepleted mantle formed by SAM–ANT spreading before the ridge–trench collision and (2) magma formed during back-arc spreading following the ridge–trench collision.

Conclusions

The South Sandwich forearc peridotites range from harzburgites, through transitional peridotites (olivine-rich with two pyroxenes) to dunites. The tectonic fabric of the harzburgites indicates that they are primarily the residues from melting at an ocean ridge or other tectonically active area. The superimposed impregnation texture in the transitional harzburgites indicates that they are the products of significant interaction between residual mantle and melt saturated in olivine or olivine + clinopyroxene. The dunites have an essentially cumulate texture. However, the (rare) presence of relict orthopyroxene, and the fact that the dunites plot within the olivine–spinel mantle array on a plot of Mg# (ol) versus Cr# (sp), indicates that they are probably the products of extreme interaction between mantle and melt.

Plots of Cr# versus TiO_2 for spinels and of Ti_{sp} versus Ti_{wr} confirm that all the South Sandwich forearc peridotites represent residual mantle that interacted with melt, the degree of interaction increasing from the harzburgites through the transitional peridotites to the dunites. The oxygen fugacity of the residual mantle end member lay close to QFM, somewhat higher than that expected for a mid-ocean ridge, which may indicate an origin at a ridge with a small subduction zone influence. The oxygen fugacity of the melt end member is at least QFM + 2. This high value, coupled with high Cr#, indicates that the reacting melts had the composition of depleted island arc tholeiites. The geometry of the region, coupled with thermal considerations, favours an origin for the South Sandwich forearc peridotites as residual mantle from the early East Scotia Sea spreading centre that was infiltrated by melts from the South Sandwich volcanic arc and then exposed in the forearc by tectonic erosion.

There are significant similarities between the South Sandwich forearc peridotites and the Mariana (Conical Seamount) forearc peridotites. Both have an inferred two-stage origin of more ocean-ridge-like residual mantle infiltrated by, and reacting with, more arc-like melts. The precise natures of the two end members are different in the two areas, however. In the South Sandwich case, the mantle protolith has a transitional (ocean ridge to island arc) character suggesting an origin at a ridge distal from, but still influenced by, a subduction zone. In the Mariana equivalent, the mantle protolith has an ocean ridge character suggesting an origin at a ridge that existed before subduction began. In the South Sandwich case, the interacting magma is of island arc tholeiite character, typical of a 'normal' island arc. In the Mariana equivalent, the interacting magma is of boninitic character, typical of supra-subduction zone magmatism associated with subduction initiation. These differences thus reflect differences in the mode of subduction initiation and subsequent evolution of the two terranes.

The South Sandwich TFI peridotites are variably serpentinised lherzolites–harzburgites that exhibit textures indicating that they represent tectonised, slightly residual mantle that has been infiltrated by, and reacted with, melt. Plots of Cr# versus TiO_2 (spinel) and of Ti_{sp} versus Ti_{wr} demonstrate that the residual mantle end member was a slightly depleted or fertile mantle with an oxygen fugacity around QFM, possibly slightly high for a mid-ocean ridge. The reacting melt had a still higher oxygen fugacity of at least QFM + 1.5. This high oxygen fugacity of the reacting melt, coupled with the close association with vesicular lavas, may indicate that the reacting melt carried a small subduction component, i.e. was transitional between MORB and IAT. This interpretation is consistent with an origin as a mantle protolith formed at the slow-spreading SAM–ANT Ridge, which interacted with magma generated at a small spreading centre at the southernmost edge of the South Sandwich back-arc basin.

The general conclusion is thus that forearc peridotites may carry geochemical signatures of origins as melt residues from one tectonic event interacting with magmas from a second event. These signatures can potentially be used to interpret the tectonic evolution of complex forearc terranes.

Acknowledgements We acknowledge the contribution of Ian Hamilton, who first worked on these rocks as part of his Ph.D. thesis. We also thank Pete Hill (Edinburgh), Chris Ottley (Durham), Ian Slipper (Greenwich) and Andy Tindle (Open University) for analytical assistance, and Paul Robinson and Riccardo Vannucci for their constructive reviews. The work was carried out as part of NERC Antarctic Special Topic Grant GST 021114.

References

Allan JF (1994) Cr-spinel in depleted basalts from the Lau Basin back-arc: petrogenetic history from Mg–Fe crystal–liquid exchange. In: Hawkins J, Parson L, Allan J et al. Proc ODP Sci Results 135. College Station, Texas (Ocean Drilling Program), pp 565–583

Arai S (1992) Chemistry of chromian spinel in volcanic rocks as a potential guide to magma chemistry. Min Mag 56: 173–184

Arai S (1994) Characterisation of spinel peridotites by olivine–spinel compositional relationships: review and interpretation. Chem Geol 113: 191–204

Ballhaus C, Berry RF, Green DH (1991) High pressure experimental calibration of the olivine–orthopyroxene–spinel oxygen barometer: implications for the oxidation state of the mantle. Contrib Mineral Petrol 197: 27–40

Barker PF (1995) Tectonic framework of the East Scotia Sea. In: Taylor B (ed) Backarc basins: tectonics and magmatism. Plenum Press, New York, pp 281–314

Barker PF, Burrell J (1977) The opening of Drake Passage. Mar Geol 25: 15–34

Barker PF, Hill IA (1981) Back-arc extension in the Scotia Sea. Philos Trans R Soc Lond A300: 249–262

Barker PF, Lawver LA (1988) South American–Antarctic plate motion over the past 50 Myr, and the evolution of the South American Antarctic Ridge. Geophys J R Astron Soc 94: 377–386

Bloomer SH (1983) Distribution and origin of igneous rocks from the landward slopes of the Mariana Trench: implications for its structure and evolution. J Geophys Res 88: 7411–7428

Bloomer SH, Hawkins JW (1983) Gabbroic and ultramafic rocks from the Mariana trench: an island arc ophiolite. In: Hayes DE (ed) The tectonic and geological evolution of the Southeast Asian seas and islands (Part 2). Am Geophys Union Geophys Monogr Ser 27: 294–317

Bodinier J-L, Merlet C, Bedini RM, Simien F, Memaidi M, Garrido CJ (1996) Distribution of niobium, tantalum, and other highly incompatible elements in the lithospheric mantle: the spinel paradox. Geochim Cosmochim Acta 60: 545–550

Bonatti E, Michael PJ (1989) Mantle peridotites from continental rifts to ocean basins to subduction zones. Earth Planet Sci Lett 91: 297–311

Dick HJB, Bullen T (1984) Chromian spinel as a petrogenetic indicator in abyssal and alpine-type peridotites and spatially associated lavas. Contrib Mineral Petrol 86: 54–76

Edwards SJ, Malpas J (1996) Melt–peridotite interactions in shallow mantle at the East Pacific Rise: evidence from ODP Site 895 (Hess Deep). Min Mag 60: 191–206

Edwards SJ, Falloon TJ, Malpas J, Pederson RB (1996) A review of the petrology of harzburgites at Hess Deep and Garrett Deep: implications for mantle processes beneath segments of the East Pacific Rise. In: MacLeod CJ, Tyler PA, Walker CL (eds) Tectonic, hydrothermal and biological segmentation of Mid Ocean Ridges. Geol Soc Lond Spec Publ 118: 143–156

Fryer P, Pearce JA (1992) Introduction to the scientific results of Leg 125. In: Fryer P, Pearce JA, Stokking LB et al. (eds) Proc ODP Sci Results 125. Ocean Drilling Program, College Station, Texas, pp 3–11

Gruau G, Bernard-Griffiths J, Lécuyer C (1998). The origin of U-shaped rare earth patterns in ophiolite peridotites: assessing the role of secondary alteration and melt/rock reaction. Geochim Cosmochim Acta 62: 3545–3560

Hamilton IW (1989) Geophysical investigations of subduction-related processes in the Scotia Sea. PhD Thesis, University of Birmingham

Hussong DM, Uyeda S (1981) Tectonic processes and the history of the Mariana arc: a synthesis of the results of Deep Sea Drilling Project Leg 60. In: Hussong DM, Uyeda S et al. (eds) Init Repts DSDP 60. US Govt Printing Office, Washington, pp 909–929

Ishii T (1985) Dredged samples from the Ogasawara forearc seamount or "Ogasawara Paleoland"–"forearc ophiolite". In: Nasu N, Kobayashi K, Uyeda S, Kushiro I, Kagami H (eds) Formation of active ocean margins. Terra Scientific Publications, Tokyo, pp 307–342

Ishii T, Robinson PT, Maekawa H, Fiske R (1992) Petrological studies of peridotites from diapiric serpentinite seamounts in the Izu–Ogasawara–Mariana forearc, Leg 125. In: Fryer P, Pearce JA, Stokking LB et al. (eds) Proc ODP Sci Results 125, Ocean Drilling Program, College Station, Texas, pp 445–486

Johnson KTM, Dick HJB, Shimizu N (1990) Melting in the oceanic upper mantle: an ion microprobe study of diopsides in abyssal peridotites. J Geophys Res 95: 2661–2678

Livermore R, McAdoo D, Marks K (1994) Scotia Sea tectonics from high-resolution satellite gravity. Earth Planet Sci Lett 123: 255–268

Kelemen PB, Dick HJB, Quick JE (1992) Formation of harzburgite by pervasive melt/rock reaction in the upper mantle. Nature 358: 635–641

Kelemen PB, Shimizu N, Salters VJM (1995) Extraction of mid-ocean ridge basalt from the upwelling mantle by focused flow of melt in dunite channels. Nature 375: 747–753

Maury RC, Defant MJ, Joron J-L (1992) Metasomatism of the sub-arc mantle inferred from trace elements in Philippine xenoliths. Nature 360: 661–663

Nell J, Wood BJ (1991) High temperature electrical measurements and thermodynamic properties of Fe_3O_4–$FeCr_2O_4$–$MgCr_2O_4$–$FeAl_2O_4$ spinels. Am Mineral 76: 405–426

Niu, Y (1997) Mantle melting and melt extraction processes beneath ocean ridges: evidence from abyssal peridotites. J Petrol 38: 1047–1074

Parkinson IJ, Arculus RJ (1999) Redox state of subduction zones: insights from arc peridotites. Chem Geol 160: 409–423

Parkinson IJ, Pearce JA (1998) Peridotites from the Izu–Bonin–Mariana forearc (ODP Leg 125): evidence for mantle melting and melt–mantle interaction in a supra-subduction zone setting. J Petrol 39: 1577–1618

Parkinson IJ, Pearce JA, Thirlwall MF, Johnson KTM, Ingram G (1992) Trace element geochemistry of peridotites from the Izu–Bonin–Mariana forearc, Leg 125. In: Fryer P, Pearce JA, Stokking LB et al. (eds) Proc ODP Sci Results 125. Ocean Drilling Program, College Station, Texas, pp 487–506

Pearce JA, Parkinson IJ (1993) Trace element models for mantle melting: application to volcanic arc petrogenesis. In: Pritchard HM, Alabaster T, Harris NBW, Neary CR (eds) Magmatic processes and plate tectonics. Geol Soc Lond Spec Publ 76: 373–403

Pearce JA, Baker PE, Harvey PK, Luff IW (1995) Geochemical evidence for subduction fluxes, mantle melting and fractional crystallization beneath the South Sandwich island arc. J Petrol 36: 1073–1109

Pouchou JL, Pichoir F (1985) ''PAP'' procedure for improved quantitative analysis. Microbeam Anal 20: 104–105

Saunders AD, Tarney J (1979) The geochemistry of basalts from a back-arc spreading centre in the East Scotia Sea. Geochim Cosmochim Acta 43: 555–572

Sobolev AV, Danyushevsky LV (1994) Petrology and geochemistry of boninites from the north termination of the Tonga Trench: constraints on the generation conditions of primary high-Ca boninite magmas. J Petrol 35: 1183–1212

Takahashi E (1980) Thermal history of lherzolite xenoliths – I. Petrology of lherzolite xenoliths from the Ichinomegata crater, Oga peninsula, northeast Japan. Geochim Cosmochim Acta 44: 1643–1658

van der Laan SR, Arculus RJ, Pearce JA, Murton BJ (1992) Petrography, mineral chemistry and phase relations of the basement boninite series of Site 786, Izu–Bonin forearc. In: Fryer P, Pearce JA, Stokking LB et al. (eds) Proc ODP Sci Results 125. Ocean Drilling Program, College Station, Texas, pp 171–201

Vanneste LE, Larter RD (1997) Subduction erosion of the South Sandwich forearc. Trans Am Geophys Union 78: F716

Wood BJ, Virgo D (1989) Upper mantle oxidation state: ferric iron contents of harzburgite spinels by ^{57}Fe Mössbauer spectroscopy and resultant oxygen fugacities. Geochim Cosmochim Acta 53: 1277–1291

Zhou M-F, Robinson PT, Malpas J, Li Z (1996) Podiform chromitites in the Luobusa ophiolite (Southern Tibet): implications for melt–rock interaction and chromite segregation in the upper mantle. J Petrol 37: 3–21